



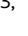



# XIAP promotes melanoma growth by inducing tumour neutrophil infiltration

Mila Daoud<sup>1,2,3,†</sup> , Pia Nora Broxtermann<sup>1,2,3,†</sup>, Fabian Schorn<sup>1,2,3</sup>, J Paul Werthenbach<sup>1,2,3</sup>, Jens Michael Seeger<sup>1,2,3</sup>, Lars M Schiffmann<sup>1,3,4</sup>, Kerstin Brinkmann<sup>5</sup> , Domagoj Vucic<sup>6</sup> , Thomas Tüting<sup>7</sup> , Cornelia Mauch<sup>8</sup>, Dagmar Kulms<sup>9,10</sup>, Paola Zigrino<sup>8</sup>  & Hamid Kashkar<sup>1,2,3,\*</sup> 

## Abstract

Elevated expression of the X-linked inhibitor of apoptosis protein (XIAP) has been frequently reported in malignant melanoma suggesting that XIAP renders apoptosis resistance and thereby supports melanoma progression. Independent of its anti-apoptotic function, XIAP mediates cellular inflammatory signalling and promotes immunity against bacterial infection. The pro-inflammatory function of XIAP has not yet been considered in cancer. By providing detailed *in vitro* analyses, utilising two independent mouse melanoma models and including human melanoma samples, we show here that XIAP is an important mediator of melanoma neutrophil infiltration. Neutrophils represent a major driver of melanoma progression and are increasingly considered as a valuable therapeutic target in solid cancer. Our data reveal that XIAP ubiquitylates RIPK2, involve TAB1/RIPK2 complex and induce the transcriptional up-regulation and secretion of chemokines such as IL8, that are responsible for intra-tumour neutrophil accumulation. Alteration of the XIAP-RIPK2-TAB1 inflammatory axis or the depletion of neutrophils in mice reduced melanoma growth. Our data shed new light on how XIAP contributes to tumour growth and provides important insights for novel XIAP targeting strategies in cancer.

**Keywords** melanoma; neutrophil; RIPK2; TAB1; XIAP

**Subject Categories** Cancer; Immunology; Signal Transduction

**DOI** 10.15252/embr.202153608 | Received 12 July 2021 | Revised 21 March 2022 | Accepted 31 March 2022 | Published online 19 April 2022

**EMBO Reports (2022) 23: e53608**

## Introduction

Cutaneous melanoma is a devastatingly aggressive malignancy arising through the transformation of melanocytes. If detected early, surgical excision with appropriate margins yields a favourable prognosis. Undetected tumour lesions however can grow and progress to invasive disease with a much less favourable course. Genetic, functional and biochemical studies suggested apoptosis resistance as one of the major drivers of melanoma progression (Soengas & Lowe, 2003). Elevated expression of the X-linked inhibitor of apoptosis protein (XIAP) has been frequently associated with melanoma progression in patients (Emanuel *et al*, 2008; Hiscutt *et al*, 2010; Ayachi *et al*, 2019) and several previous studies indicated that XIAP targeting can promote susceptibility to apoptosis in melanoma cells (Lecis *et al*, 2010; Seeger *et al*, 2010b; Hornle *et al*, 2011). Together, these studies highlighted the therapeutic value of XIAP targeting strategies in melanoma treatments.

X-linked inhibitor of apoptosis protein consists of three Baculovirus IAP Repeat (BIR 1–3) motifs promoting protein–protein interaction and a Really Interesting New Gene (RING) domain (Liston *et al*, 1996; Uren *et al*, 1996; Farahani *et al*, 1997) which confers ubiquitin ligase (E3) activity (Yang *et al*, 2000; Nakatani *et al*, 2013). Initial studies identified BIR2, BIR3 and the linker element between BIR1 and BIR2 domains as the responsible caspase binding/inhibitory elements of XIAP rendering apoptosis resistance (Eckelman *et al*, 2006). Independently, XIAP has been long known to induce NFκB activation and MAP kinase signalling by involving TGFβ-activated kinase 1 (TAK1) (Yamaguchi *et al*, 1999) upon direct interaction with the TAK1 binding protein (TAB1) via its BIR1 domain (Lu *et al*, 2007). Further studies showed that XIAP interacts via its BIR2 domain with the kinase domain of the receptor-interacting protein kinase 2 (RIPK2), an adaptor of the NOD

1 Faculty of Medicine and University Hospital of Cologne, Institute for Molecular Immunology, University of Cologne, Cologne, Germany  
 2 Faculty of Medicine and University Hospital of Cologne, Center for Molecular Medicine Cologne (CMMC), University of Cologne, Cologne, Germany  
 3 Cologne Excellence Cluster on Cellular Stress Responses in Aging-Associated Diseases (CECAD), University of Cologne, Cologne, Germany  
 4 Faculty of Medicine and University Hospital of Cologne, Department of General, Visceral, Cancer and Transplant Surgery, University of Cologne, Cologne, Germany  
 5 The Walter & Eliza Hall Institute of Medical Research (WEHI) and Department of Medical Biology, University of Melbourne, Melbourne, Vic., Australia  
 6 Department of Early Discovery Biochemistry, Genentech, South San Francisco, CA, USA  
 7 Laboratory of Experimental Dermatology, Department of Dermatology, University Hospital Magdeburg, Magdeburg, Germany  
 8 Faculty of Medicine and University Hospital of Cologne, Department of Dermatology and Venereology, University of Cologne, Cologne, Germany  
 9 Department of Dermatology, Experimental Dermatology, TU-Dresden, Dresden, Germany  
 10 National Center for Tumor Diseases Dresden, TU-Dresden, Dresden, Germany  
 \*Corresponding author. Tel: +49 221 47884091; E-mail: h.kashkar@uni-koeln.de  
 †These authors contributed equally to this work

inflammatory signalling machinery (NF $\kappa$ B activation; Krieg *et al*, 2009; Heim *et al*, 2020). XIAP-mediated NF $\kappa$ B activation was shown to involve its RING-mediated ubiquitin ligase activity, characterising XIAP as an E3 ligase involved in cellular inflammatory signalling (Damgaard *et al*, 2012; Takeda *et al*, 2014). Conventional (Harlin *et al*, 2001) and conditional (Andree *et al*, 2014) ablation of *Xiap* in mice, however, did not cause phenotypic alteration indicating that the physiological role of XIAP as an anti-apoptotic protein may be redundant or limited in scope (Kashkar, 2010; Seeger *et al*, 2010a; Silke & Vucic, 2014). XIAP-deficient mice, however, were shown to be susceptible to bacterial infection identifying XIAP as a central mediator of innate immunity (Bauler *et al*, 2008; Prakash *et al*, 2010; Andree *et al*, 2014).

Previous studies addressing the role of XIAP in melanoma mainly considered XIAP as an anti-apoptotic factor enabling cancer cells to resist cytotoxic anti-cancer therapy (Kashkar, 2010; Fulda & Vucic, 2012). These studies mainly involved tumour cell culture or xenograft mouse models and were therefore unable to explore the role of XIAP-mediated inflammatory signalling in cancer and its effect on tumour cell crosstalk with the tissue environment or immune system. Here, we show that XIAP is an important component of tumour-associated inflammation and melanoma growth by performing detailed *in vitro* studies and by utilising two independent *in vivo* mouse melanoma models. Our data indicate that the specific interactions with TAB1 and RIPK2 are decisive for XIAP in order to induce chemokine secretion in tumour cells. In particular, the secretion of interleukin-8 (IL8) by melanoma cells and the subsequent neutrophil infiltration of melanomas are shown to be dependent on XIAP expression.

## Results and Discussion

### Lack of XIAP in B16 mouse melanoma reduces tumour growth without enhancing tumour cell apoptosis

In order to examine the role of XIAP in melanoma progression, we employed a syngeneic melanoma mouse model involving immune-competent mice bearing B16 cutaneous melanomas (Coutelle *et al*, 2014; Witt *et al*, 2015; Schiffmann *et al*, 2020). Two XIAP knock-out (XIAP<sup>KO</sup>) B16 melanoma cell lines were generated using CRISPR/Cas9 with two independent single guide RNAs (sgRNAs) targeting the *Xiap* gene at different sites (Fig 1A). Upon subcutaneous injection, both wild-type and XIAP<sup>KO</sup> B16 cells formed palpable tumours in mice while tumour volumes were significantly reduced in XIAP<sup>KO</sup> tumour xenografts (Fig 1B). We did not detect any increase in apoptotic cell death in XIAP<sup>KO</sup> B16 tumours (staining of active caspase-3; Fig 1C). Apoptotic propensity of XIAP<sup>KO</sup> B16 cells was also not altered in culture when cells were exposed to TNF or TRAIL (Fig EV1A and B). Furthermore, no alteration of cellular proliferation was observed in XIAP<sup>KO</sup> B16 melanoma cells (Fig EV1C). These observations suggested that the reduced tumour size in XIAP<sup>KO</sup> B16 melanoma cells was not caused by alterations in tumour cell proliferation/death.

### XIAP mediates IL8 secretion in melanoma by involving TAB1 and RIPK2

Independent of its anti-apoptotic function, XIAP promotes inflammatory signalling and cytokine secretion, which can potentially

support tumour growth (Coussens & Werb, 2002). Cytokine/chemokine transcripts were investigated in two independent XIAP<sup>KO</sup> cell lines versus wild type B16 (Appendix Table S1 and S2). This analysis revealed that transcripts of C-X-C motif chemokine ligand (CXCL) family including CXCL1 (also called melanoma growth stimulating activity  $\alpha$  (MGSA- $\alpha$ ), neutrophil-activating protein 3 (NAP-3) or keratinocytes-derived chemokine (KC) in mice) and CXCL10 were reduced in XIAP<sup>KO</sup> B16 melanoma cells (Figs 1D and EV1D).

CXCL family members such as CXCL1 and IL8 have been frequently described in human melanoma progression and their expression has been tightly associated with tumour growth and Breslow thickness (Cesati *et al*, 2020). In line, knock-down of XIAP using specific siRNAs (Seeger *et al*, 2010a, 2010b) or XIAP knock-out by CRISPR/Cas9 technology in human melanoma cells consistently reduced IL8 secretion in all tested human tumour cells under steady-state conditions (Figs 1E and F and EV1E). IL8 secretion can also be induced under inflammatory condition such as exposure to tumour necrosis factor (TNF; Abreu-Martin *et al*, 1995). XIAP knock-down or knock-out could also reduce TNF-induced IL8 secretion in the majority of tested cells; however, it failed to completely diminish IL8 secretion in response to TNF (Fig EV1F and G). These observations suggest that TNF promotes IL8 secretion not exclusively by involving XIAP. Independently, overexpression of myc-tagged XIAP (myc-XIAP), but not myc-XIAP<sup>ARING</sup> lacking the Ub-ligase activity, required for XIAP-mediated inflammatory signalling (Silke & Vucic, 2014), prominently induced transcriptional up-regulation and secretion of IL8 in HEK293T cells (Fig 1G and H, and Appendix Table S3). In line with previous studies (Hofer-Warbinek *et al*, 2000; Goncharov *et al*, 2018), these data indicated that the elevated XIAP expression which is frequently seen in melanoma (Emanuel *et al*, 2008) can alone promote IL8 secretion. These results, however, do not exclude possible involvement of further extrinsic cues within the melanoma environment which could additionally boost IL8 production.

In addition to the RING domain, the deletion of BIR1 and BIR2, but not BIR3, efficiently diminished IL8 production in HEK293 cells ectopically expressing myc-XIAP (Fig EV2A). BIR1 and BIR2 interaction with TAB1 and RIPK2, respectively, have previously been shown to induce NF $\kappa$ B activation (Yamaguchi *et al*, 1999; Lu *et al*, 2007). Our data showed that ectopically expressed myc-XIAP in HCT116 (Fig EV2B) or endogenously expressed XIAP in BLM melanoma cells (Fig 2A) interacts with RIPK2 and TAB1. Further analysis showed that GFP-XIAP co-localises with TAB1 and RIPK2 (Fig 2B). The co-localisation of GFP-XIAP with TAB1 was dependent on BIR1 domain. BIR2 domain was required for the co-localisation of GFP-XIAP with RIPK2 (Fig EV2C). Upon binding, XIAP was previously shown to ubiquitylate RIPK2 (Damgaard *et al*, 2012). In a cell-free ubiquitylation assay (Albert *et al*, 2020) using recombinant XIAP and RIPK2 proteins, our data also showed that XIAP efficiently ubiquitylated RIPK2 (Fig 2C). RIPK2 ubiquitylation was markedly reduced in human and mouse melanoma cells lacking XIAP, together indicating that XIAP in melanoma ubiquitylates RIPK2 (Fig 2D).

Ubiquitylated RIPK2 serves as binding platform for TAK1/TAB1 complex which initiates inflammatory signalling ultimately leading to IL8 secretion (Hofer-Warbinek *et al*, 2000; Hasegawa *et al*, 2008; Heim *et al*, 2020). In order to examine the role of TAB1 and RIPK2 in XIAP-mediated IL8 secretion, we generated HCT116 cell lines

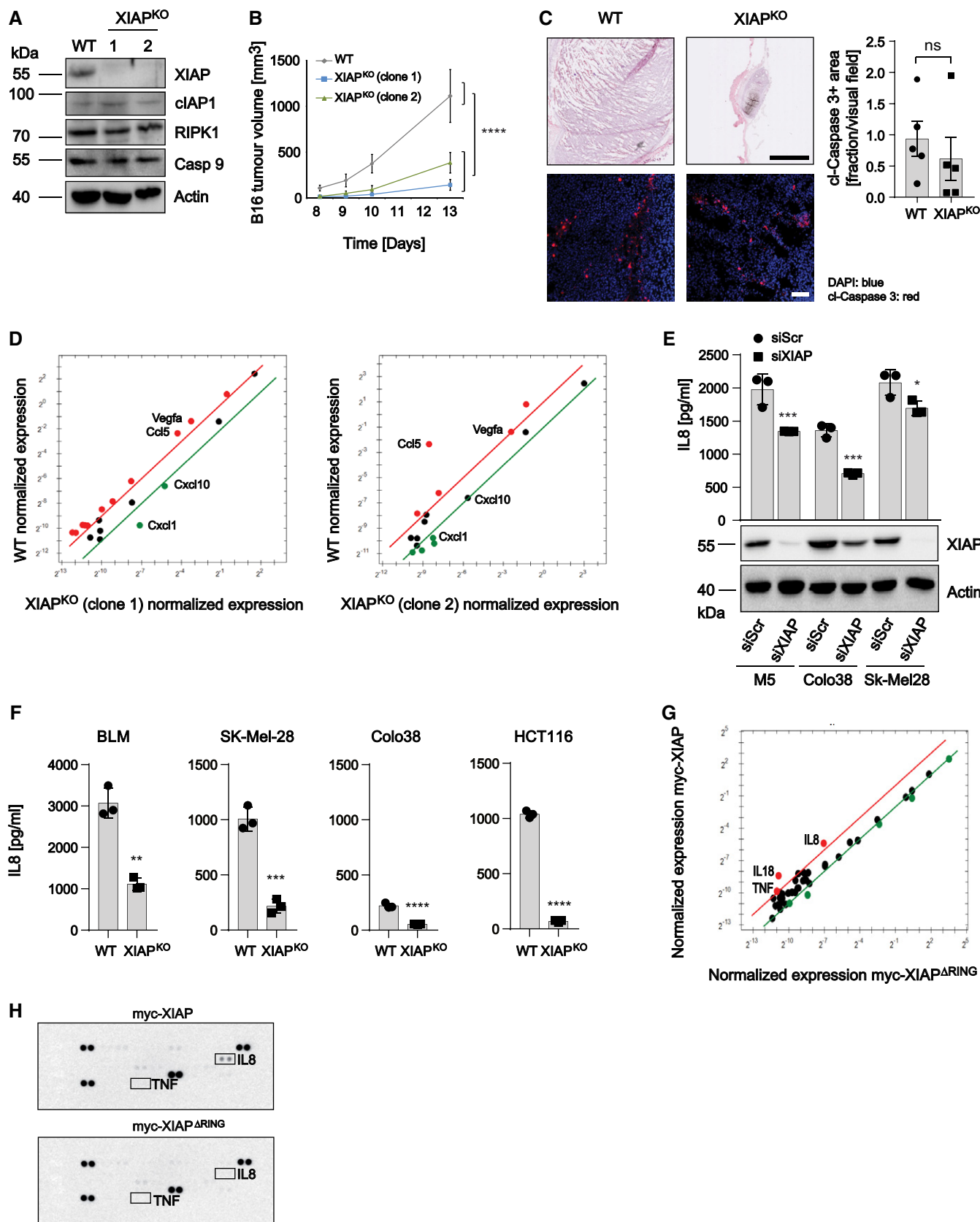


Figure 1.

**Figure 1. XIAP promotes tumour growth without interfering with tumour cell apoptosis.**

- A Western blot analysis of B16F1 WT and two independent XIAP<sup>KO</sup> cell lines. Actin was used as a loading control.
- B Subcutaneous melanoma tumour growth in BL/6 WT mice ( $n = 5$ ) using B16F1 WT and XIAP<sup>KO</sup> (clone1 and 2). Data are mean  $\pm$  s.e.m. Two-way analysis of variance (ANOVA) followed by Dunnett's post-analysis.
- C Representative H&E (scale bar 50  $\mu$ m) and fluorescent images of cI-Caspase 3 staining in B16 WT and XIAP<sup>KO</sup> tumours. Nuclei were stained with DAPI (blue). Scale bar 100  $\mu$ m. Quantification thereof (right panel). The average of cI-Caspase 3 positive cells from 5 randomly selected areas of the tumour (5 mice per genotype) was represented. Dots represent individual mice ( $n = 5$ ). Data are presented as mean  $\pm$  s.e.m. Mann-Whitney, two-tailed test analysis.
- D qRT-PCR analysis (PrimePCR™ Assay) of different cyto-/chemokines in B16F1 WT cells plotted vs B16F1-XIAP<sup>KO</sup> cells (clone1 and 2). Samples that are at least 2-fold up-regulated are shown in red, samples that are at least 2-fold down-regulated are shown in green.
- E IL8 measurement in the supernatant of the indicated cell lines after 48 h transfection with siScr (control) or siXIAP and Western blot analysis of the corresponding cell lysates (bottom). One-way analysis of variance (ANOVA) followed by Dunnett's post-analysis.
- F IL8 measurement in the supernatant of the indicated cell lines after 24 h of seeding the cells. Unpaired  $t$ -test, two-tailed analysis.
- G qRT-PCR analysis (PrimePCR™ Assay) of different cyto-/chemokines in HEK293T cells overexpressing myc-XIAP plotted vs HEK293T cells overexpressing myc-XIAP<sup>ARINC</sup>. Samples that are at least 2-fold up-regulated are shown in red, samples that are at least 2-fold down-regulated are shown in green.
- H Human cytokines array analysis of HEK293T cells transfected with myc-XIAP or myc-XIAP<sup>ARINC</sup>. Medium was changed after 16 h and the supernatant was collected after 48 h. Pre-spotted nitrocellulose membranes were incubated with the supernatants overnight at 4°C.

Data information: In E and F, data are presented as mean  $\pm$  SD. Dots represent individual biological replicates. \* $P < 0.05$ ; \*\* $P < 0.01$ ; \*\*\* $P < 0.001$ ; \*\*\*\* $P < 0.0001$  and ns, not significant.

Source data are available online for this figure.

lacking either TAB1 or RIPK2 by using CRISPR/Cas9 gene editing. Our data showed that TAB1 or RIPK2 knock-out efficiently reduced IL8 secretion in HCT116 cells ectopically expressing myc-XIAP (Fig EV2D–F). In addition to the results obtained in the model cell line HCT116, specific knock-down of TAB1 or RIPK2 in melanoma cells BLM or SK-Mel28 efficiently reduced IL8 secretion (Fig 2E). In contrast, the knock-down of upstream signalling component NOD1 or XIAP binding partners, caspase-3 and caspase-7, did not interfere with IL8 secretion in melanoma cells (Fig EV2G). These data indicate that XIAP in melanoma cells utilises its BIR1 and BIR2 domains, involves TAB1 and RIPK2 and induces inflammatory signalling ultimately yielding IL8 secretion. Accordingly, a recently developed XIAP antagonist XB2d89, which specifically targets the BIR2 domain of XIAP (Goncharov *et al*, 2018) could efficiently block IL8 secretion in melanoma cells (Fig 2F). In contrast, previously reported IAP antagonists such as birinapant and BV6, which target BIR3 domain of XIAP, could not abolish, and even increased IL8 secretion in BLM melanoma cells (Fig 2G) presumably, by targeting cIAP1 and cIAP2 and activation of the non-canonical NF $\kappa$ B (Varfolomeev & Vucic, 2008; Goncharov *et al*, 2018).

Previous data identified XIAP as a critical component of the intracellular pathogen receptor nucleotide-binding and oligomerisation domains (NOD)1/2 signalling which was engaged upon intracellular

bacterial infection and causing IL8 secretion (Krieg *et al*, 2009; Andree *et al*, 2014). In line with these results, our data showed that the exposure of cells to the bacterial peptidoglycan muramyl dipeptide (MDP) induced IL8 secretion which was dependent on the expression of XIAP, TAB1 and RIPK2 (Fig EV2H).

**XIAP induces neutrophil infiltration and supports melanoma growth by involving TAB1 and RIPK2**

In order to study the involvement of XIAP-BIR1 and XIAP-BIR2 domains in melanoma tumour growth, we generated B16 melanoma cell lines lacking XIAP-BIR1 (XIAP<sup>ΔBIR1</sup>) or -BIR2 (XIAP<sup>ΔBIR2</sup>) domain using CRISPR/Cas9 gene editing (Fig EV3A). Similar to XIAP<sup>KO</sup>, genetic ablation of XIAP-BIR1 or XIAP-BIR2 domain markedly reduced B16 melanoma tumour growth in mice (Fig 3A). Importantly, the deletion of BIR1 domain resulted in reduced expression levels/detection of XIAP<sup>ΔBIR1</sup> protein in cell lysates. The analysis of mRNA level of XIAP however did not reveal any marked reduction in the expression level of XIAP<sup>ΔBIR1</sup> (Fig EV3B). The observed discrepancy may be caused by altered epitope accessibility for the used anti-XIAP antibodies or increased XIAP protein turnover/degradation upon ablation of BIR1 domain. In order to further evaluate our observations using XIAP<sup>ΔBIR1/2</sup> cells, we generated B16

**Figure 2. XIAP mediates IL8 secretion in melanoma by involving TAB1 and RIPK2.**

- A Western blot analysis of cell lysates of BLM and BLM-XIAP<sup>KO</sup> cells (input) and XIAP-IP. Data are representative of two experiments.
- B Confocal microscopic analysis of transfected HCT116 cells with GFP-XIAP for 16 h and stained for TAB1 or RIPK2 (red). Nuclei were stained with DAPI (blue). Scale bar 20  $\mu$ m.
- C Cell-free ubiquitylation assay of recombinant GST-RIPK2 by Flag-XIAP after addition of respective E1/E2 and recombinant ubiquitin. Poly-ubiquitylated RIPK2 and XIAP were detected by Western blotting.
- D Western blot analysis of cell lysates of BLM, BLM-XIAP<sup>KO</sup>, SK-Mel28, SK-Mel28-XIAP<sup>KO</sup>, B16, and B16-XIAP<sup>KO</sup> cells (input) and RIPK2-IP. Poly-ubiquitin is detected using anti-ubiquitin antibody.
- E IL8 measurement in the supernatant of transfected BLM (left panel) or SK-Mel28 (right panel) cells with siScr (control), siXIAP, siTAB1 or siRIPK2 after 48 h. Western blot analysis of the respective cell lysates of BLM cells (left bottom) or SK-Mel28 cells (right bottom) transfected with the indicated siRNA.
- F IL8 measurement in the supernatant of BLM or SK-Mel28 treated with 2  $\mu$ M d89 (BIR2 antagonist) or DMSO as a negative control for 24 h.
- G IL8 measurement in the supernatant of BLM or SK-Mel28 treated with 20  $\mu$ M birinapant (Bir), 2  $\mu$ M BV6 (both BIR3 antagonist) or DMSO as a negative control for 24 h.

Data information: In E, F and G, dots represent individual biological replicates. Data are presented as mean  $\pm$  SD. Unpaired  $t$ -test, two-tailed test analysis (F) or One-way analysis of variance (ANOVA) followed by Dunnett's post-analysis (E and G). \* $P < 0.05$ ; \*\* $P < 0.01$ ; \*\*\* $P < 0.001$  and \*\*\*\* $P < 0.0001$ .

Source data are available online for this figure.

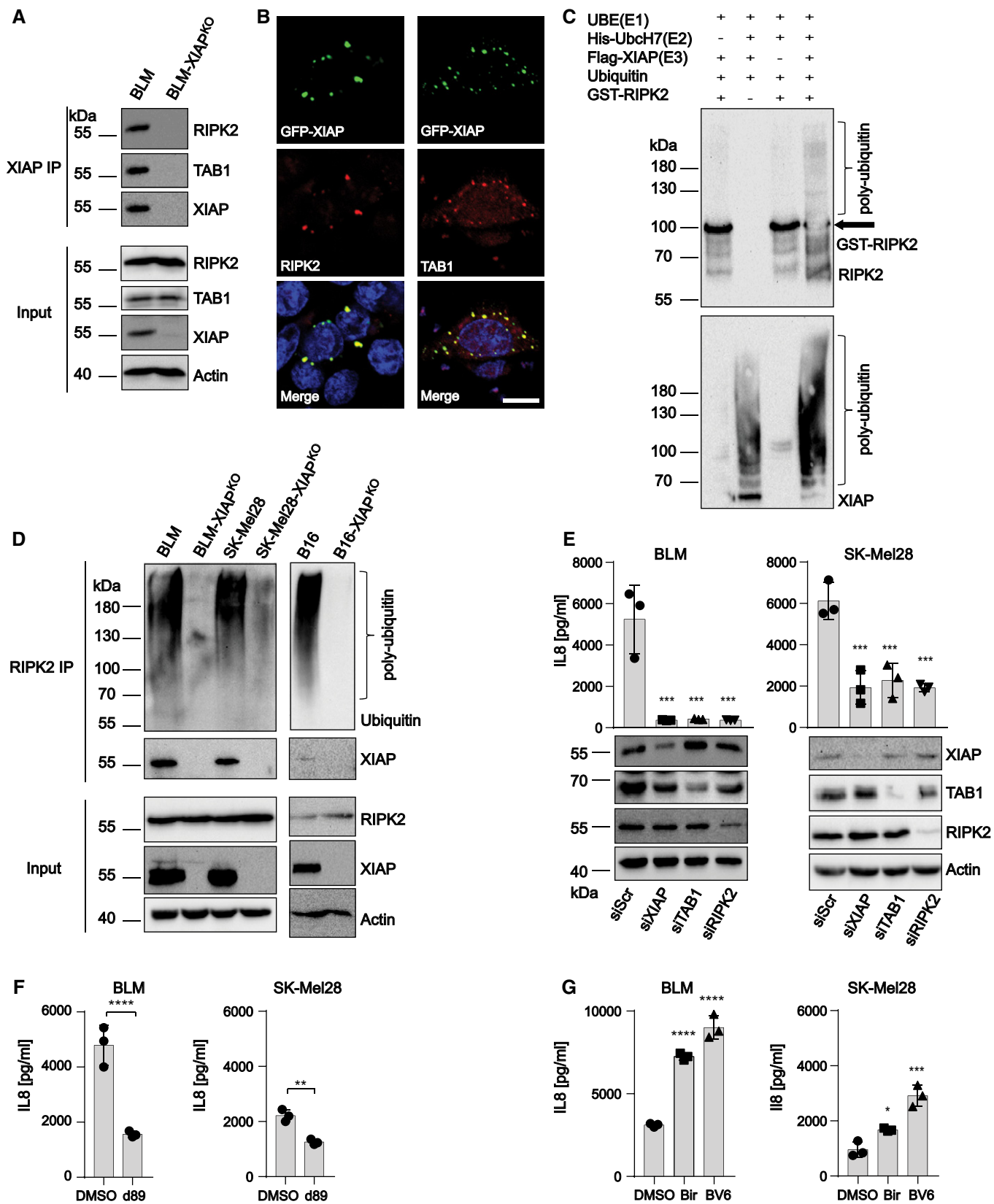
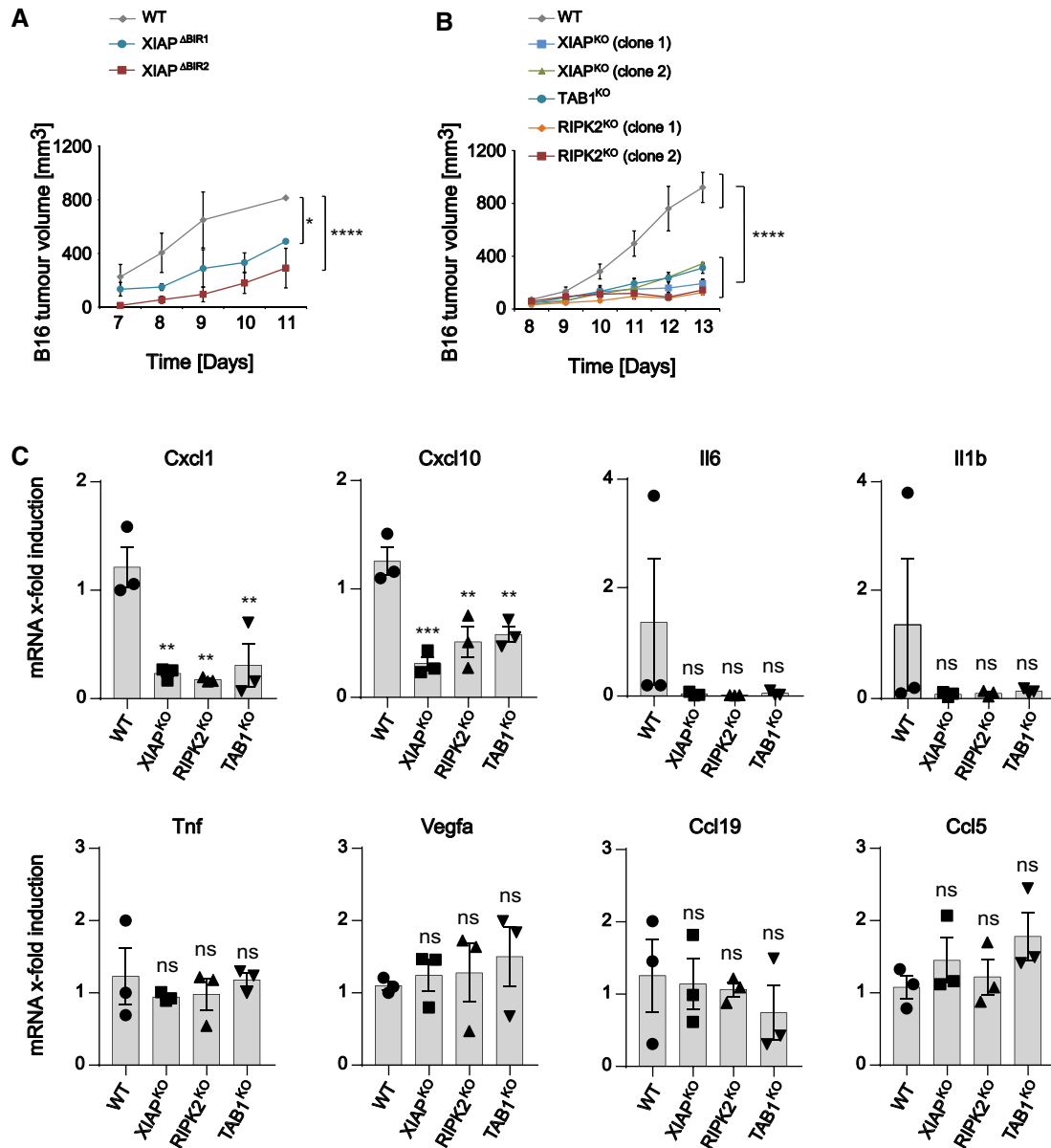


Figure 2.



**Figure 3. XIAP BIR1- and -BIR2 support melanoma growth via TAB1- and RIPK2-dependent signalling.**

A B16F1 WT, B16F1-XIAP<sup>ΔBIR1</sup> and B16F1-XIAP<sup>ΔBIR2</sup> subcutaneous melanoma tumour growth in BL/6 WT mice ( $n = 3$  each genotype).

B B16F1 WT, B16F1-XIAP<sup>KO</sup> (clone 1 and 2), B16F1-TAB1<sup>KO</sup> and B16F1-RIPK2<sup>KO</sup> (clone 1 and 2) subcutaneous melanoma tumour growth in BL/6 WT mice ( $n = 5$  each genotype).

C qRT-PCR analysis of different cytokines/chemokines in the indicated melanoma tumours in mice. Dots represent individual mice ( $n = 3$ ). Data are presented as mean  $\pm$  SD. One-way analysis of variance (ANOVA) followed by Dunnett's post-analysis.

Data information: In A and B data are mean  $\pm$  s.e.m.; two-way analysis of variance (ANOVA) followed by Dunnett's post-analysis. \* $P < 0.05$ ; \*\* $P < 0.01$ ; \*\*\* $P < 0.001$ ; \*\*\*\* $P < 0.0001$  and ns, not significant.

melanoma cell lines lacking TAB1 (TAB1<sup>KO</sup>) or RIPK2 (RIPK2<sup>KO</sup>) (Fig EV3C). Similar to XIAP<sup>ΔBIR1/2</sup> cells, ablation of TAB1 or RIPK2 reduced B16 melanoma tumour growth in mice (Fig 3B). We were not able to detect any increase in active caspase-3 staining in these tumours (Fig EV3D). Cell death/proliferation was also not altered in cultured tumour cells (Incucyte analysis) (Fig EV3E and F). Similar to the data obtained from cultured melanoma cells (Fig 1), lower levels of Cxcl1 (KC) and Cxcl10 were consistently detected in mouse

melanoma tumours lacking XIAP, TAB1 or RIPK2 (Fig 3C). These data collectively indicate that XIAP supports melanoma growth by activating down-stream inflammatory signalling cascades involving TAB1 and RIPK2.

Members of the CXCL chemokine family, including CXCL1 and CXCL8 (IL8), represent mediators of neutrophil chemotaxis and promote melanoma growth and progression (Payne & Cornelius, 2002; Jensen *et al*, 2012). Melanoma infiltration by neutrophils is

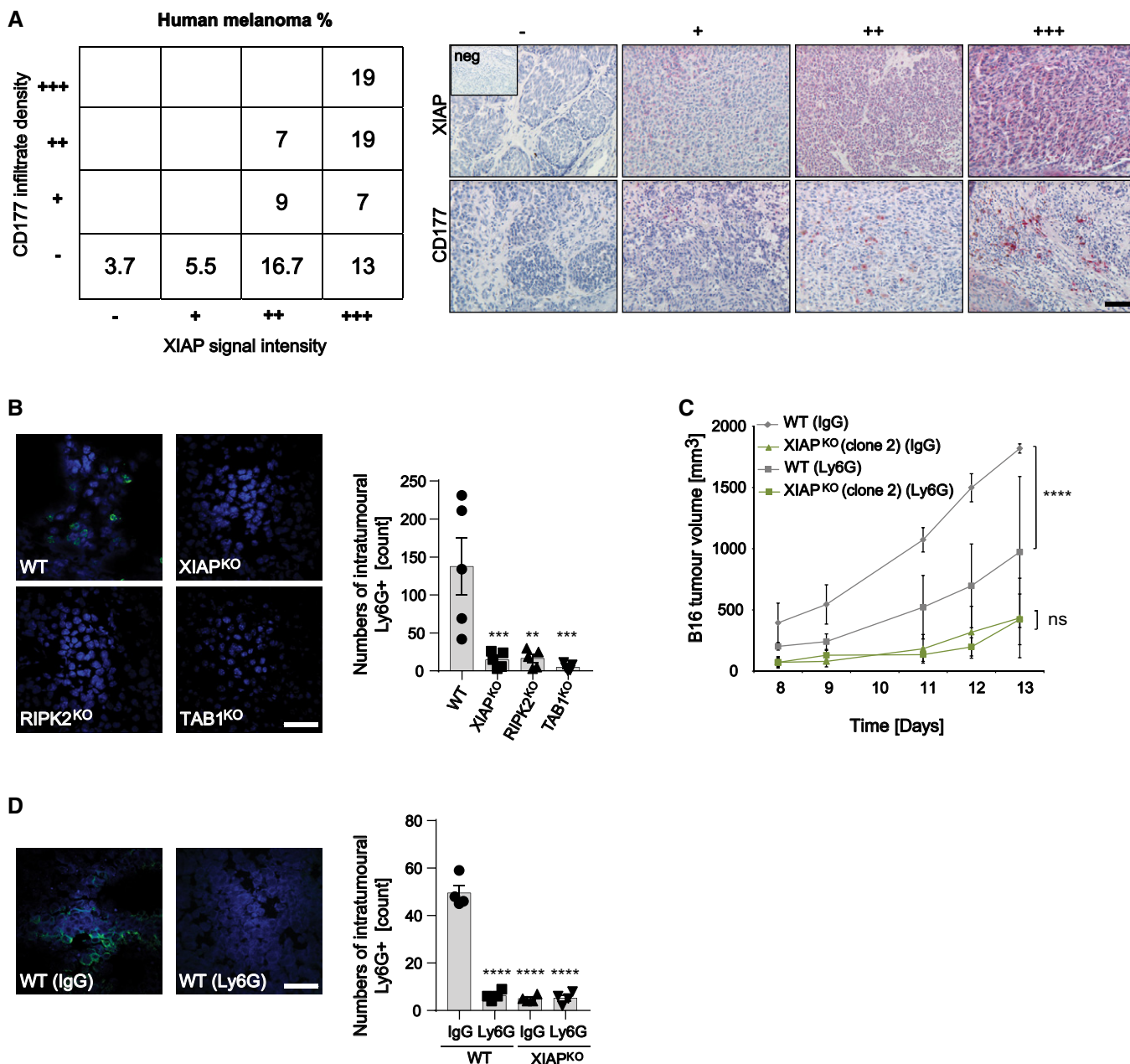


**Figure 4. XIAP-RIPK2-TAB1 axis supports neutrophil infiltration and melanoma growth in B16 mouse melanoma.**

**A** Intensities of CD177 and XIAP immunostainings in tumour sections from 55 patients were visually scored. The numbers of melanomas with different intensities were plotted into the table as a percentage of the total. Specific staining intensity for XIAP and CD177, corresponding to relative amounts of infiltrated neutrophils, was arbitrarily set as the following: -, not expressed; +, low; ++, moderate; and +++, strong expression. Representative IHC pictures (right panel). Scale bar 100  $\mu$ m.

**B** Representative IF (neutrophils staining) in B16F1 WT, XIAP<sup>KO</sup>, TAB1<sup>KO</sup> or RIPK2<sup>KO</sup> tumours (Scale bar 50  $\mu$ m) and quantification of Ly6G<sup>+</sup> cells. The sum of Ly6G-positive cells from 5 randomly selected areas of the tumour (5 mice per genotype) was represented. Dots represent individual mice ( $n = 5$ ).

**C** B16F1 WT, XIAP<sup>KO</sup> (clone 2) subcutaneous melanoma tumour growth in BL/6 WT mice ( $n = 5$ ). Mice were intra-peritoneal injected with IgG antibody as a negative control or Ly6G antibody 1 day prior to the subcutaneous injection of the B16F1 WT or XIAP<sup>KO</sup> cells. Data are mean  $\pm$  s.e.m. Two-way analysis of variance (ANOVA) followed by Dunnett's post-analysis.

**D** Representative IF (neutrophils) scale bar 50  $\mu$ m and quantification of Ly6G<sup>+</sup> cells in tumours from C. The sum of Ly6G-positive cells from 5 randomly selected areas of the tumour (4 mice per genotype) was represented. Dots represent individual mice ( $n = 4$ ).

Data information: In B and D, data are presented as mean  $\pm$  s.e.m. One-way analysis of variance (ANOVA) followed by Dunnett's post-analysis. \*\* $P < 0.01$ ; \*\*\* $P < 0.001$ ; \*\*\*\* $P < 0.0001$  and ns, not significant.

associated with poor prognosis (Bodey *et al*, 1996; Damgaard *et al*, 2012) and hence the neutrophil count serves as an important tumour biomarker (Masucci *et al*, 2019). Analysis of neutrophil infiltration (CD177 expression) in tumour samples derived from melanoma patients showed that increased XIAP expression in tumour cells is tightly associated with intra-tumour neutrophil infiltration (Fig 4A, Appendix Table S4).

To examine whether XIAP expression in tumour cells can induce chemotaxis of neutrophils, we first performed a granulocyte migration assay using XIAP-deficient or -proficient HCT116, BLM and SK-Mel28 cells. Our data showed that XIAP knock-out significantly reduced granulocyte migration in all tested cell lines (Fig EV4A). Furthermore, granulocyte migration was efficiently blocked when IL8 was neutralised in the supernatants of XIAP-proficient cells (Fig EV4B). Exogenously added IL8, in turn, could efficiently restore granulocyte migration in assays using XIAP-deficient cells (Fig EV4C). These data demonstrated that XIAP-induced IL8 secretion can promote neutrophil chemotaxis.

We next examined whether the expression of XIAP, TAB1 or RIPK2 is important for the intra-tumoural neutrophil infiltration in murine B16 melanomas. Lack of XIAP, RIPK2 or TAB1 significantly reduced neutrophil infiltration (Figs 4B and EV4D), but not other tested immune cells (Appendix Fig S1), in B16 tumours. Notably, in contrast to cultured melanoma cells, cytokine expression analysis of mouse tumour bulks showed that the ablation of XIAP, TAB1 or RIPK2 led to the reduction of Il6 and Il1b in addition to the Cxcl1 and Cxcl10 (Fig 3C). As XIAP<sup>KO</sup>, TAB1<sup>KO</sup> or RIPK2<sup>KO</sup> tumours are barely infiltrated with myeloid cells, the observed reduction in the total amount of Il6 or Il1b in these tumours may due to the reduced appearance of intra-tumoural immune cells.

Whether the reduced neutrophil infiltration entailed the reduced tumour growth in XIAP<sup>KO</sup> B16 melanoma tumours was studied by inducing experimental neutrophil depletion in mice using Ly6G specific antibodies. Neutrophil depletion using Ly6G specific antibodies in mice efficiently reduced neutrophil infiltration and B16 tumour growth (Figs 4C and D, and EV4E). In contrast to wild-type B16 melanoma, exposure to Ly6G neutralising antibodies did not alter the growth of XIAP<sup>KO</sup> B16 melanoma further indicating that XIAP is required for neutrophil tumour infiltration and melanoma growth.

Our studies involving model cell lines, melanoma cells, human melanoma tissue samples and B16 cutaneous melanoma mouse model conclusively showed that XIAP supports melanoma growth by inducing tumour cell inflammatory signalling and chemokine

secretion that promotes neutrophil infiltration and tumour growth. In order to further substantiate our results, we used the *Hgf-Cdk4*<sup>R24C</sup> melanoma mouse model, which more faithfully imitates the genetic and biologic evolution of human melanoma (Tormo *et al*, 2006; Giebeler *et al*, 2017). XIAP-deficient mice (*Xiap*<sup>KO</sup>) (Andree *et al*, 2014) were crossed with *Hgf-Cdk4*<sup>R24C</sup> mice and spontaneous melanoma development was investigated. Both *Hgf-Cdk4*<sup>R24C</sup>*Xiap*<sup>fl/fl</sup> and *Hgf-Cdk4*<sup>R24C</sup>*Xiap*<sup>KO</sup> mice developed back skin melanomas starting at the age of 26 weeks. We were not able to detect a marked alteration in tumour initiation (tumour number) (Fig EV5A) but the sum tumour size was significantly reduced in *Hgf-Cdk4*<sup>R24C</sup>*Xiap*<sup>KO</sup> mice (Fig 5A). Furthermore, the lack of XIAP slightly improved median survival in melanoma-prone *Hgf-Cdk4*<sup>R24C</sup>*Xiap*<sup>KO</sup> compared to *Hgf-Cdk4*<sup>R24C</sup>*Xiap*<sup>fl/fl</sup> mice (Fig EV5B), together indicating that XIAP is not required for melanoma tumour initiation but supports melanoma growth and progression in *Hgf-Cdk4*<sup>R24C</sup> melanoma mouse model.

With the purpose of further enhancing melanomagenesis and to establish a more synchronised tumour initiation/progression in mice, we used neonatal carcinogen (7,12-dimethylbenz[*a*]anthracene (DMBA)) treatment, which is characterised by inducing many primary melanomas in the skin growing rapidly within the first 3 months of life in *Hgf-Cdk4*<sup>R24C</sup> melanoma mouse model (Tormo *et al*, 2006). The data obtained revealed that *Xiap* ablation reduced the number and the size of melanoma tumours after carcinogen treatment (Fig 5B–D). We could not detect any alteration in melanoma initiation and detected almost similar numbers of tumours below 10 mm<sup>2</sup> of size (Fig 5C). The appearance of tumours with a size beyond 10 mm<sup>2</sup> was however markedly reduced in *Hgf-Cdk4*<sup>R24C</sup>*Xiap*<sup>KO</sup> mice. Analysis of cytokine/chemokine expression in melanomas derived from *Hgf-Cdk4*<sup>R24C</sup>*Xiap*<sup>KO</sup> versus *Hgf-Cdk4*<sup>R24C</sup> mice (Appendix Table S5, Appendix Table S6 and Appendix Table S7) revealed reduced expression of CXCL family members upon XIAP ablation (Fig 5E). Neutrophil infiltration in mouse melanomas was significantly reduced in *Hgf-Cdk4*<sup>R24C</sup>*Xiap*<sup>KO</sup> mice already in early small melanomas but also in tumours at later stages (Figs 5F and G and EV5C and D). Similar to the data obtained in B16 melanoma (Fig 1), loss of XIAP in *Hgf-Cdk4*<sup>R24C</sup> melanomas did not increase tumour cell apoptosis (caspase-3 activation) (Fig EV5E). These data indicated that XIAP is not required for the process of malignant transformation in *Hgf-Cdk4*<sup>R24C</sup> mouse melanoma but importantly supports tumour growth by promoting neutrophil infiltration.

**Figure 5. XIAP supports tumour growth by promoting neutrophil infiltration in *Hgf-Cdk4*<sup>R24C</sup> mouse melanoma.**

- A Sum tumour size in *Hgf-Cdk4*<sup>R24C</sup>*Xiap*<sup>fl/fl</sup> and *Hgf-Cdk4*<sup>R24C</sup>*Xiap*<sup>KO</sup> mice at 38 weeks of age. Dots represent sum of all tumours size in an individual mouse. Data are presented as mean ± s.e.m. Unpaired t-test, two-tailed test analysis.
- B Representative images of back skin of the DMBA-treated *Hgf-Cdk4*<sup>R24C</sup>*Xiap*<sup>fl/fl</sup> and *Hgf-Cdk4*<sup>R24C</sup>*Xiap*<sup>KO</sup> mice at 8 weeks of age. Arrows indicate individual tumour. Scale bar 5 mm.
- C Number of tumours in the DMBA-treated mice at 8 weeks of age (*n* = 3). Dots represent tumours having a range size of 0–10, 10–40 or > 40 mm<sup>2</sup> in an individual mouse. Data are presented as mean ± s.e.m. Two-way analysis of variance (ANOVA) followed by Sidak's post-analysis.
- D Tumour size in the DMBA-treated *Hgf-Cdk4*<sup>R24C</sup>*Xiap*<sup>fl/fl</sup> and *Hgf-Cdk4*<sup>R24C</sup>*Xiap*<sup>KO</sup> mice at 8 weeks of age (*n* = 3). Dots represent an individual tumour. Data are presented as mean ± SD. Mann–Whitney, two-tailed test analysis.
- E qRT–PCR analysis (PrimePCR™ Assay) of different cyto-/chemokines in *Hgf-Cdk4*<sup>R24C</sup>*Xiap*<sup>fl/fl</sup> mice plotted vs 3 independent *Hgf-Cdk4*<sup>R24C</sup>*Xiap*<sup>KO</sup> mice. Samples that are at least 2-fold up-regulated are shown in red, samples that are at least 2-fold down-regulated are shown in green.
- F, G Representative IHC staining of neutrophils in small (early time points) (F) and large (late time points) (G) tumours. Scale bar 100 μm (upper panel) and 10 μm (lower panel). Arrows show neutrophils.

Data Information: \**P* < 0.05; \*\**P* < 0.01 and ns, not significant.



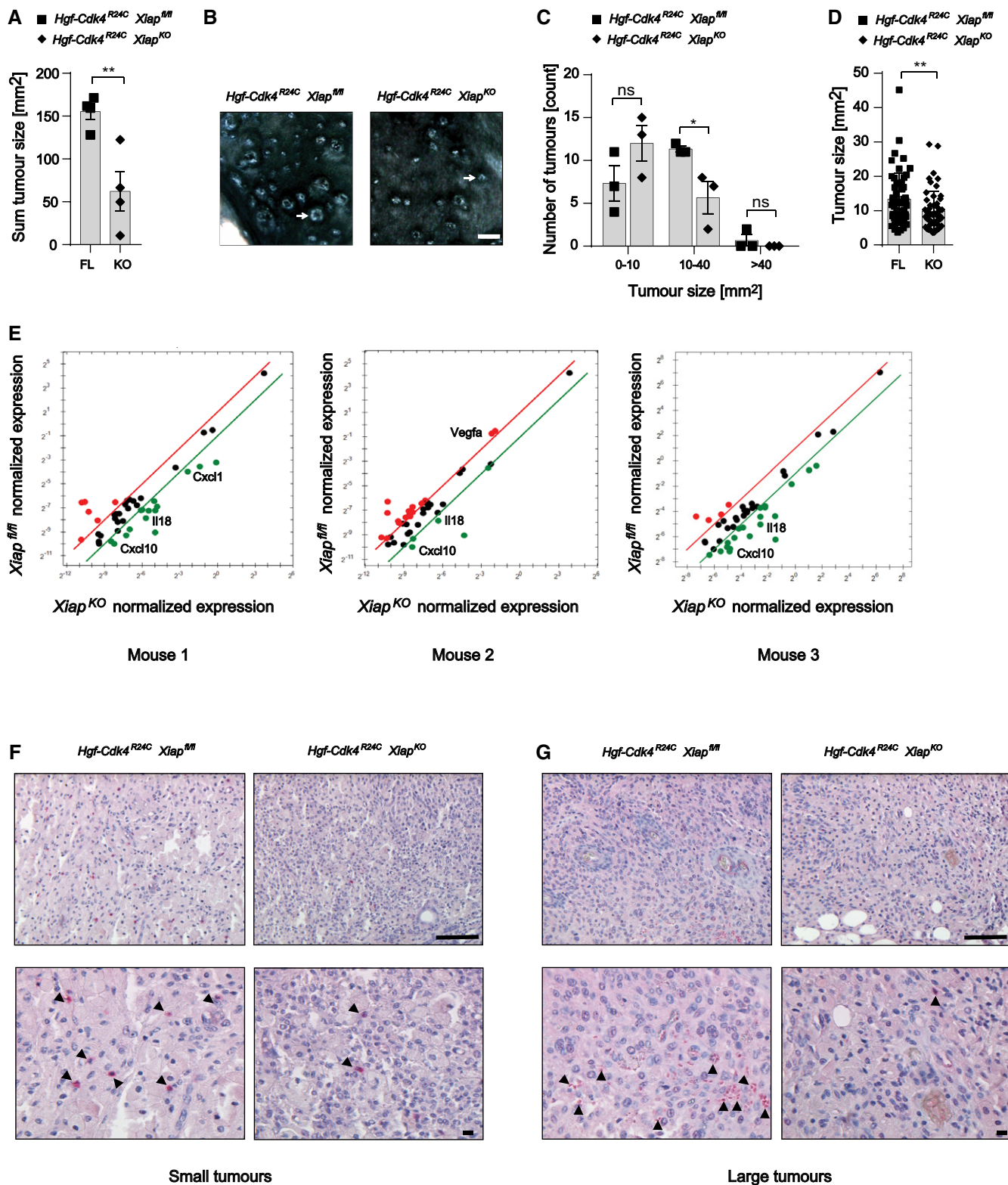


Figure 5.

Tumour immune-cell infiltrating is a hallmark of cancer (Hanahan & Weinberg, 2011). Neutrophils represent 50–70% of the myeloid-derived white circulating cells in human blood and are

mainly involved in the human innate immunity against invading pathogens (Borregaard, 2010). They also represent the most of inflammatory cells in solid tumours with a high intra-tumour

density that are increasingly identified as key drivers of tumour progression (Mantovani *et al*, 2009) and valuable therapeutic targets in cancer (Gregory & Houghton, 2011). Accordingly, strategies aiming at targeting non-cancer-cell component of the tumours, in particular, by pharmacologically blocking chemokine signalling (*e.g.* blocking IL8 and CXCL1) or neutrophil-derived substances have been viewed as valuable therapeutic options for cancer (Gregory & Houghton, 2011; Masucci *et al*, 2019). By discovering one of the central signalling machineries in tumour cells which drives tumour neutrophil infiltration, our study proposes XIAP-RIPK2-TAB1 signalling complex as a novel and valuable therapeutic target for cancer therapy. In particular, the recent discovery and the development of small molecules that efficiently and specifically interfere with XIAP-RIPK2 interaction and disrupt cellular inflammatory signalling (Nachbur *et al*, 2015; Goncharov *et al*, 2018; Hrdinka *et al*, 2018) will provide valuable tools to diminish neutrophil-mediated tumour growth.

## Material and Methods

### Generation of stable knock-out cell lines

Gene knock-out in cell lines was carried out by using CRISPR/Cas9 gene editing (Fritsch *et al*, 2019). Cells were transfected with the designed oligonucleotide sgRNAs (purchased from Eurofins Genomics or designed and purchased from Sigma-Aldrich as indicated in Appendix Table S8), cloned into the pSpCas9(BB)-2A-GFP (PX458) vector (a gift from F. Zhang; Addgene plasmid 48138). Transfected cells, expressing GFP, were sorted according to their expression with a BD Influx™ cell sorter (BD Biosciences). GFP-positive cells were cultured for 4 days, followed by diluting cells to a single cell suspension plated on a 96-well plate. Next, the plated cells were grown in an appropriate colony size and analysed via Western blot and sequencing.

### Subcutaneous injection of B16F1 cell lines

BL/6 mice were received from the CECAD animal facility. At age of 8–12 weeks, mice were subcutaneously injected into the flank region with 100  $\mu$ l of  $1 \times 10^7$  cells/ml of B16F1 WT cells or *in vitro* generated B16F1 KO cells. Tumour growth was measured in 2 dimensions every second day. When reaching a tumour size of 15 mm in diameter, the mice were sacrificed. Tumour volume was calculated as length  $\times$  width<sup>2</sup>  $\times$   $\pi/6$  (Witt *et al*, 2015; Schiffmann *et al*, 2020). For *in vivo* experiments, the majority of analyses included at least 3 mice per group in a simple experiment. Mouse experiments were repeated in independent experimental replicates. Sample size estimate was based on our previous studies and the approval by the German Regulations for Welfare of Laboratory Animals.

### Intra-peritoneal injection (IP) of antibodies

Intra-peritoneal injection of IgG2a (InVivo plus, clone C1.18.4) or Ly6G (InVivo plus, clone 1A8) was performed 1 day prior to the injection of tumour cells until the end of the experiment in a dose of 100  $\mu$ g antibody in 100  $\mu$ l PBS per mouse per day (Coffelt *et al*, 2015; Schiffmann *et al*, 2019; Szczerba *et al*, 2019).

### Hgf-Cdk4<sup>R24C</sup> mice

*Xiap*<sup>KO</sup> and *Hgf-Cdk4*<sup>R24C</sup> mice were described previously (Andree *et al*, 2014). For carcinogen-induced tumour growth, neonates were treated with 160 nmol DMBA in acetone 4 days after birth. Development of melanocytic neoplasms and other skin tumours in both, untreated and DMBA-treated animals, was monitored weekly. Nevi and melanomas were counted and tumour size was measured in two dimensions using a calliper (tumour size is given in mm<sup>2</sup>). When a single tumour reached a size of approx. 1.5 cm, or the sum of tumours was exceeding 3.0 cm in diameter, the animals were sacrificed. Animals were housed in the animal care facility of the University of Cologne under standard pathogen-free conditions with a 12 h light/dark schedule and provided with food and water ad libitum. Animal experiments were performed following German Regulations for Welfare of Laboratory Animals and with approval by LANUV NRW (NRW authorisation for generation of the line 84-02.04.2015.A471 and 84-02.04.2016.A012 to analyse tumour development).

### Immunofluorescence staining of isolated mice tumours

Tumours were embedded in O.C.T. compound, Tissue-Tek, and stored at  $-80^{\circ}\text{C}$ . To analyse neutrophils infiltration, cryosections (10  $\mu$ m) were fixed in acetone, washed with PBS, blocked with 10% normal goat serum in addition to 5% BSA and stained with a monoclonal rat anti-mouse Ly-6G (1:200, #551459, BD Pharmingen). Secondary Alexa Fluor 488 goat anti-rat antibody (1:1,000, #A11006, life technologies) was used. To analyse active caspase 3, cryosections (10  $\mu$ m) were fixed in 10% PFA, washed with PBS, blocked with 10% normal goat serum and stained with a polyclonal rabbit anti-cleaved caspase-3 (Asp 175) (1:200, #9661, Cell Signaling). Secondary Alexa Fluor 594 (#A11012) or 647 (#A21244) goat anti-rabbit antibody (1:1,000, life technologies) were used (Gunther *et al*, 2020). Immune cell phenotyping was performed using IHC Antibody Sampler Kit (#37495, Cell Signaling). All antibodies were used in a 1:200 dilution. Secondary Alexa Fluor 488 goat anti-rabbit antibody (1:1,000, #A11008, life technologies) was used. Tumour cells nuclei were stained with 4,6-diamidin-2-phenylindol (DAPI). Imaging was conducted on a motorised inverted Olympus IX81 microscope (CellR Imaging Software) or Fluoview FV1000 confocal microscope (Olympus GmbH) was used (objective: Olympus PlanApo, 60 $\times$ /1.40 oil,  $\infty/0.17$ ). Cl-Caspase-3<sup>+</sup> areas were calculated using ImageJ software (<http://imagej.nih.gov/ij>). Number of Ly-6G<sup>+</sup> infiltrates were counted manually (Schiffmann *et al*, 2019) or Ly-6G<sup>+</sup> areas were calculated using ImageJ software.

### H&E staining of isolated mice tumours

Cryosections from B16 tumours were incubated for 10 min in tap water, 3.5 min in Haematoxylin, shortly washed with tap water followed by 15 min incubation with tap water and then 1 min in demineralised water. Next, sections were incubated for 1 min in Eosin followed by dehydration in a serial of ethanol dilutions and Xylol. Sections were fixed with Entellan. Stained tumours were scanned using a Hamamatsu Slide scanner (S360) and analysed using the imaging software NDP.view 2.

### Immunohistochemistry staining of isolated mice tumours

Parraffin sections were deparaffinised in alcohol series, washed with demineralised water followed by bleaching which was done as following: 20 min incubation with 30% H<sub>2</sub>O<sub>2</sub> and 0.5% KOH at 37°C, 20-s incubation with 1% acetic acid and washed with demineralised water. Antigen unmasking was done using Citrate buffer (pH: 6) with 0.05% Tween 20, heated 4× in the microwave and cooled down at RT for 20 min. Next, blocking was done using 10% BSA in TBS for 30 min. After that, sections were stained with a monoclonal rat anti-mouse Ly-6G primary antibody (1:500, #551459, BD Pharmingen) diluted in 1% BSA and TBS at 4°C overnight. Chromogen staining was done as following: incubation with goat anti-rat biotin-conjugated secondary antibody (1:500, #112-065-003, JacksonImmunoResearch) for 45 min at RT, 3x washing with TBS for 5 min, 15 min incubation with Alkaline phosphatase (Fa.DCS #AD000RP) followed by 3× washing with TBS. Sections were incubated with Chromogen (Fast Red Substrate Pack, Fa. BioGenex #HK182-5KE) for 5 min. Nuclear staining was done by incubating the sections with haematoxylin for 1 min, followed by 3x washing in warm tap water and finally washed with demineralised water.

### Immunohistochemistry in human samples

Paraffin-embedded sections (7 µm) of human melanoma specimens from patients diagnosed at the University Hospital of Cologne were obtained using a Thermo Shandon Finesse Microtome, collected on microscope slides (Gerhard Menzel GmbH) and dried overnight at 37°C. Sections were deparaffinised by incubation of the slides in xylene (20 min) followed by a graded alcohol series (1 min each): isopropyl alcohol, 96% EtOH, 75% EtOH, aqua bidest.

Antigen retrieval was performed using Target Retrieval System pH 6.0 (TRS, Dako) in a preheated water bath at 95°C for 20 min. Slides were cooled at RT before immersing in wash buffer for the next step. Sections were washed three times in TBS blocked for 1 h with 10% BSA in TBS. Primary antibodies diluted in TBS, 1% BSA were added to the sections and incubated overnight at 4°C in a humidified chamber. The following antibodies were used: rabbit-anti-CD177 (1:400, #PA5-83575, Invitrogen) and rabbit-anti-XIAP (1:100, #ab21278, Abcam). After 2x5 min washes in TBS, bound antibodies were detected using the DAKO REAL kit (K5005) and fast red (#HK182-5KE, Fa. BioGenex) as a substrate. Nuclei were counterstained with haematoxylin solution for 1min (Shandon). Stained sections were viewed and recorded using Leica DM 4000B microscope (Leica) equipped with Diskus program version 4.50.1638 – #393. Expression of XIAP and amount of CD177-positive cells were qualitatively estimated according to the intensity of specific staining and were arbitrarily set as the following: –, not expressed; +, low; ++, moderate; +++, strong.

### Ethics approval

Human materials were obtained according to the study protocol conformed to the ethical guidelines of the 1975 Declaration of Helsinki and were approved by the Ethics Committee of the Medical Faculty of the University of Cologne (Approval No. 21-1006). Informed consent has been obtained.

### Granulocytes migration

Granulocytes were isolated from human peripheral blood using the isolation of mononuclear cells from human peripheral blood by density gradient centrifugation protocol (Miltenyi Biotec) according to the manufacturer's instruction. HCT116 WT, HCT116-XIAP<sup>KO</sup>, BLM WT, BLM-XIAP<sup>KO</sup>, SK-Mel28 WT or SK-Mel28-XIAP<sup>KO</sup> were seeded on a 24 well plate (150000 cells per well in 600 µl medium) (Millicell-24 Merck). After 48 h, 1 × 10<sup>6</sup> granulocytes were plated onto the semipermeable membrane (5 µm) and migrated cells were measured after 1 h using flow cytometry analysis. αIL8 antibody (0.2, 0.4 µg/ml, R&D systems) were added to the WT medium and rh-IL8 (2, 4 ng/ml, R&D systems) were added to the KO medium after 47 h of seeding the cells. 1 h later, 1 × 10<sup>6</sup> granulocytes were plated onto the semipermeable membrane (5 µm), and migrated cells were measured after 1 h using flow cytometry analysis.

### Western blot

Whole cell lysates were prepared using either CHAPS lysis buffer (10 mM HEPES pH 7.4, 150 mM NaCl, 1% (w/v) CHAPS, protease inhibitor; complete Mini, Roche), or RIPA lysis buffer (1% Triton X-100, 150 mM NaCl, 50 mM Tris pH 7.4, 0.1% SDS, 0.5% Na-deoxycholat, protease inhibitor; complete Mini, Roche). Collected cell pellets were resuspended in 1 pellet volume lysis buffer, incubated for 20 min on ice, followed by centrifugation at 20,000 g for 20 min at 4°C. Protein concentrations of cell lysates were measured using a Pierce BCA Protein Assay (Thermo Fisher Scientific) according to the manufacturer's instructions. Proteins were separated by SDS-PAGE and transferred to a nitrocellulose membrane (Amersham Protean, GE). Proteins were stained with antibodies against XIAP (#610763, BD Biosciences or # M044-3, MBL), TAB1 (#3226, Cell Signaling), TAB1 (#3387, ProSci), RIPK2 (#4142, Cell Signaling), β-Actin (#A5441, Sigma), cIAP1 (#ALX-803-335, Enzo), RIPK1 (#51-6559GR, BD Biosciences), Capase-9 (#ab2014, Abcam), Caspase-3 (#9665, Cell Signaling), Caspase 7 (#9494, Cell Signaling), p-RIPK2 (#4364, Cell Signaling), c-Myc HRP (#ab62928, Abcam), Ubiquitin (#3936, Cell Signaling) and Caspase-8 mouse-specific (#4927, Cell Signaling). Secondary antibodies included goat anti-rabbit IgG conjugated to horseradish peroxidase (HRP) (#7074, Cell Signaling), goat anti-mouse IgG HRP (#A4416, Sigma), goat anti-mouse IgG light chain HRP (#115-035-174, Jackson Immuno Research) and goat anti-rat IgG (H + L) HRP (#031470, Invitrogen). Membranes were developed using a ChemiDoc MP Imaging System (BioRad).

### Immunoprecipitation

HCT116 cells were transfected with respective constructs for 24 h. Cells were collected and lysed using IP-lysis buffer from µMACS c-myc Isolation Kit (Miltenyi Biotec), incubated 20 min on ice and centrifuged at 20,000 g for 20 min at 4°C. Lysates were magnetically labelled with µMACS c-myc MicroBeads. Immunoprecipitation was performed according to the manufacturer's instructions and analysed by Western blot (Albert *et al*, 2020).

## Endogenous IP

Immunoprecipitation of endogenous proteins analysis was done as described previously (Albert *et al*, 2020). In brief, cells were washed with chilled PBS and centrifuged at 700 g for 3 min. The cell pellet was resuspended in lysis buffer (Miltenyi Biotec) in addition to *N*-ethylmaleimide (NEM) (Sigma-Aldrich) and 1× complete protease inhibitor cocktail (Roche) followed by 30 min incubation on ice and centrifugation for 20 min at 20,000 g at 4°C. Supernatant was collected and incubated first 1 h with a respective antibody against XIAP (#14334, Cell Signaling) at 4°C on a rotating wheel followed by overnight incubation with Protein A/G Plus agarose beads (sc-2003, Santa Cruz). Beads were washed 3× with PBST (PBS + 0.1% Tween 20).

Immunoprecipitation of endogenous ubiquitylated RIPK2 was carried out as described above. The cell pellet was resuspended in RIPA buffer (1% Triton, 150 mM NaCl, 50 mM Tris, 1% SDS, 0.5% deoxycholate) in addition to *N*-ethylmaleimide (NEM) (Sigma-Aldrich) and 1× complete protease inhibitor cocktail (Roche) followed by 30-min incubation on ice and centrifugation for 20 min at 20,000 g at 4°C. SDS concentration was diluted to 0.1% SDS prior to antibody incubation. Lysates were incubated first 1 h with a respective antibody against RIPK2 (#4142, Cell Signaling) at 4°C on a rotating wheel followed by overnight incubation with Protein A/G Plus agarose beads (sc-2003, Santa Cruz). Beads were washed 3× with PBST (PBS + 0.1% Tween 20).

## In vitro cell-free ubiquitylation assay

The following recombinant proteins were used: UBE1, His-UbcH7, ubiquitin (Boston Biochem), flag-XIAP (BPS Bioscience) and GST-RIPK2 (technical novusbio). Ubiquitin assay was performed in 10× E3 ubiquitin ligase buffer (Enzo) and 10× activation buffer (Enzo) for 2 h at 37°C followed by 5 min on ice. The reaction was done using 2 µg ubiquitin, 1 µg E2 (UbcH7), 0.4 µg E1 (UBE1), 0.5 µg substrate (RIPK2) and 0.78 µg E3 (XIAP) in a total amount of 25 µl reaction.

## Cell proliferation assays

Cell proliferation assay of generated CRISPR/Cas9 cell lines was assessed *in vitro* either by using CellTrace™ CFSE Cell Proliferation Kit for flow cytometry (Thermo Fisher Scientific) or by Incucyte Live-Cell-Analysis according to the manufacturer's instructions. Cell proliferation was measured after 24 h and 72 h.

## Immunofluorescence

Immunofluorescence analysis was performed as described previously (Albert *et al*, 2020). In brief, HCT116 or HeLa cells were seeded on coverslips in 12-well plate and transfected with GFP-XIAP for 16 h. Cells were washed with PBS and subsequently fixed with 3% paraformaldehyde in PBS for 20 min. Cells were blocked and permeabilised with blocking buffer (0.1% saponin (Carl Roth), 3% BSA (Carl Roth) in PBS) for 30 min and later incubated with primary antibodies for TAB1 (1:100, Cell Signaling) or RIPK2 (1:100, Cell Signaling) in a humid chamber overnight at 4°C. After incubation, coverslips were washed with washing buffer (0.1% saponin in

PBS) three times and incubated with secondary antibody goat anti-rabbit Alexa Fluor 568 (1:500, Thermo Fisher Scientific) for 1 h at room temperature. Subsequently, cells were stained with 300 nM DAPI (Molecular Probes) for 10 min and washed three times and embedded with mowiol overnight. For imaging, Fluoview FV1000 confocal microscope (Olympus GmbH) was used (objective: Olympus PlanApo, 60×/1.40 oil, ∞/0.17).

## RNA isolation

RNA was isolated using either RNeasy Kit (Qiagen) according to the manufacturer's instructions or standard phenol-chloroform-method (Chomczynski & Sacchi, 1987). Cells were resuspended in TRIzol® (Ambion, Life Technologies) and afterwards homogenised using QIAshredder columns (Qiagen). Chloroform was added to the homogenate of cells, incubated on ice and centrifuged to separate the homogenate into a lower organic layer containing DNA and proteins, an interphase and an upper aqueous layer containing the RNA. Aqueous layer was collected; RNA was precipitated by adding isopropanol, washed with 70% ethanol and resolved in nuclease-free water. RNA was quantified by measuring at wavelength 260 nm with a spectral photometer (NanoDrop®) and stored at −80°C. To purify RNA from single- and double-stranded DNA, RNA was digested with DNaseI (Thermo Scientific) according to the manufacturer's instructions. Level of purity was checked by agarose gel electrophoresis.

## Reverse transcription and quantitative PCR (qRT-PCR)

RevertAid™ Premium First Strand cDNA Synthesis Kit (Thermo Fisher) was used to synthesize the cDNA from the RNA with oligo dT-primers according to the manufacturer's instructions. qRT-PCR was performed with specific primers (Appendix Table S9). Light-Cycler® SYBR-Green I Mix (Roche Applied Sciences) was used with a 96-well-plate Multicolor Real-Time PCR Detection System (iQTM5, BIO-RAD). Data were further evaluated as previously described (Ramakers *et al*, 2003), and target gene expression was normalised to the reference gene Actin.

## PrimePCR™ assay

To determine the transcription level of different cyto- and chemokines, Bio-Rad PrimePCR™ Assay Plate Cytochemokines Tier 1 H96 or M96 was used. The assay was performed according to the manufacturer's instructions. Data analysis was carried out with Bio-Rad PrimePCR analysis software.

## Enzyme-linked immunosorbent assay (ELISA)

Human melanoma cells were seeded on 12-well plate and transfected with siRNA alone for 48 h or additionally treated with TNF 20 ng/ml (Biomol) for 8 h. HEK293T, HCT116-TAB1<sup>KO</sup> and HCT116-RIPK2<sup>KO</sup> cells were seeded on 12-well plate and transfected with indicated plasmids for 16 h. Medium was changed and collected after 24 h. HCT116 cells were treated with L18-MDP 1 µg/ml (InvivoGen) for 24 h. Medium was collected and frozen at −20°C. Human melanoma cells were treated with Birinapant 20 µM (Biozol), BV6 2 µM (Universal Biologicals) or XB2d89 (d89) 2 µM (Genentech, USA). Analysis of secreted IL8 was performed using

human CXCL8/IL8 DuoSet ELISA (R&D Systems) according to the manufacturer's instructions.

### Cell death assay

20,000 cells were seeded on 96-well plate and treated with either 100 ng/ml TNF (R&D), 50 ng/ml TRAIL (Enzo), DMSO (Roth) or 2 mM H<sub>2</sub>O<sub>2</sub> (Roth) for 24 h. Treatments were done in the presence of 5 μM Sytox Green (Invitrogen). Analysis of cell death was performed using an InCyte system (SARTORIUS). Scanning was done every 1 or 2 h over 24 h with 20× magnification. Cell death was determined as Sytox positive cells and quantified with the software supplied by the manufacturer.

### Cultivation and transfection of cells

HeLa, HEK293T, HCT116, B16 cells were purchased from ATCC. HCT-XIAP<sup>KO</sup> cell line was described previously (Cummins *et al*, 2004). M5, BLM, Colo38 and SK-Mel28 cell lines were described previously (Brinkmann *et al*, 2013). HeLa, HEK293T and B16F1 cells were cultured in DMEM (Merck) supplemented with 10% FCS (Biowest), 100 μg/ml streptomycin and 100 unit/ml penicillin (Merck). HCT116 cells (human colon cancer cell line) were cultured in McCoy's 5A (Merck) supplemented with 10% FCS (Biowest). M5, BLM, Colo38 and SK-Mel28 melanoma cells were cultured in RPMI (Merck) supplemented with 10% FCS (Biowest), 100 μg/ml streptomycin, 100 unit/ml penicillin (Biochrom) and non-essential amino acids (Biochrom). Cells were routinely tested for mycoplasma contaminations by PCR. Cells were transfected with respective constructs for 16 h using Lipofectamine<sup>®</sup> 2000 (Invitrogen) or Polyethylenimin (PEI) (Polysciences Europe GmbH) according to the manufacturer's instructions. For siRNA transfection, cells were transfected with the respective siRNA for 48 h using Lipofectamine<sup>®</sup> RNAi MAX<sup>™</sup> (Invitrogen) according to the manufacturer's instructions. The following siRNA were used: siTAB1 (5'-GG AUGAGCUCUCCGUCUUUU- 3'), siRIPK2 (5'-GUAUGAUCUCUCU AAUAGA- 3'), siXIAP (5'-GGAAUAAAUGUCCAUGCTT- 3') siCaspase3 (5'-GGAAUAUCCUGGACAACATT-3'), siCaspase7 (5'-UAC CGUCCUCUCAGUAATT- 3'), siNOD1 (5'-CCCUGAGUCUUGCGU CCAA- 3') and siScr (5'-GGA UUA CUU GAU AAC GCU AUU- 3'; Gunther *et al*, 2020). siRNAs were designed and purchased from Eurofins Genomics.

### Statistical analysis

Data are presented as mean ± SD or ± s.e.m. *In vitro* experiments were repeated at least two times. The respective tests or analyses are listed in the figure's legend. Significances were indicated as \**P* < 0.05, \*\**P* < 0.01, \*\*\**P* < 0.001, \*\*\*\**P* < 0.0001; ns, not significant. GraphPad Prism 7.0 and Excel were used to analyse the data in this study.

## Data availability

This study includes no data deposited in external repositories.

**Expanded View** for this article is available online.

## Acknowledgements

We thank M. Menning, A. Manav, T. Roth, and J. Zamek for their technical assistance. We thank B. Vogelstein (Johns Hopkins University) for HCT116-XIAP<sup>KO</sup> cells (Cummins *et al*, 2004). This work was supported by the German Cancer Aid (70114685 and 70114225) (grant to HK) and German Cancer Aid (70114473) grant to PZ. The Deutsche Forschungsgemeinschaft (DFG) (KA 2853/4-1, SFB1403 (project number 414786233), SFB1218 (project number 269925409) (grant to HK). MD was supported by the graduate program in Pharmacology and Experimental Therapeutics at the University of Cologne which is supported by Bayer. Open Access funding enabled and organized by Projekt DEAL.

## Author contributions

**Mila Daoud:** Data curation; Software; Formal analysis; Validation; Investigation; Visualization; Methodology; Writing—original draft; Writing—review and editing. **Pia Nora Broxtermann:** Data curation; Software; Formal analysis; Validation; Investigation; Visualization; Methodology. **Fabian Schorn:** Investigation; Methodology. **J Paul Werthenbach:** Investigation; Methodology. **Jens Michael Seeger:** Methodology. **Lars M Schiffmann:** Methodology. **Kerstin Brinkmann:** Methodology. **Domagoj Vucic:** Resources. **Thomas Tüting:** Resources. **Cornelia Mauch:** Resources; Investigation. **Dagmar Kulms:** Resources. **Paola Zigrino:** Resources; Supervision; Validation; Investigation; Visualization; Methodology. **Hamid Kashkar:** Conceptualization; Supervision; Funding acquisition; Writing—original draft; Writing—review and editing.

In addition to the CRediT author contributions listed above, the contributions in detail are:

MD and PNB performed most experiments and data analysis. FS established *Hgf-Cdk4<sup>R24C</sup>* and *Hgf-Cdk4<sup>R24C</sup>Xiap<sup>KO</sup>* mouse melanomas. JPW generated B16<sup>ΔBIR1</sup> and B16<sup>ΔBIR2</sup> B16 cell lines and performed respective tumour analysis. JMS and LMS helped with mice injections and mouse tumour studies. KB was involved in initial studies characterising XIAP in human melanoma cells. DV and DK provided essential reagents and cell lines. TT provided *Hgf-Cdk4<sup>R24C</sup>* melanoma mouse model. CM and PZ provided analyses of tumours derived from melanoma patients. HK designed the study.

## Disclosure and competing interests statement

The authors declare that they have no conflict of interest.

## References

- Abreu-Martin MT, Vidrich A, Lynch DH, Targan SR (1995) Divergent induction of apoptosis and IL-8 secretion in HT-29 cells in response to TNF-alpha and ligation of Fas antigen. *J Immunol* 155: 4147–4154
- Albert MC, Brinkmann K, Pokrzywa W, Gunther SD, Kronke M, Hoppe T, Kashkar H (2020) CHIP ubiquitylates NOXA and induces its lysosomal degradation in response to DNA damage. *Cell Death Dis* 11: 740
- Andree M, Seeger JM, Schull S, Coutelle O, Wagner-Stippich D, Wiegmann K, Wunderlich CM, Brinkmann K, Broxtermann P, Witt A *et al* (2014) BID-dependent release of mitochondrial SMAC dampens XIAP-mediated immunity against Shigella. *EMBO J* 33: 2171–2187
- Ayachi O, Barlin M, Broxtermann PN, Kashkar H, Mauch C, Zigrino P (2019) The X-linked inhibitor of apoptosis protein (XIAP) is involved in melanoma invasion by regulating cell migration and survival. *Cell Oncol (Dordr)* 42: 319–329
- Bauler LD, Duckett CS, O'Riordan MX (2008) XIAP regulates cytosol-specific innate immunity to Listeria infection. *PLoS Pathog* 4: e1000142

- Bodey B, Bodey Jr B, Siegel SE, Luck JV, Kaiser HE (1996) Immunophenotypic characterization of human primary and metastatic melanoma infiltrating leukocytes. *Anticancer Res* 16: 3439–3446
- Borregaard N (2010) Neutrophils, from marrow to microbes. *Immunity* 33: 657–670
- Brinkmann K, Zigrino P, Witt A, Schell M, Ackermann L, Broxtermann P, Schüll S, Andree M, Coutelle O, Yazdanpanah B et al (2013) Ubiquitin C-terminal hydrolase-L1 potentiates cancer chemosensitivity by stabilizing NOXA. *Cell Rep* 3: 881–891
- Cesati M, Scatozza F, D'Arcangelo D, Antonini-Cappellini GC, Rossi S, Tabolacci C, Nudo M, Palese E, Lembo L, Di Lella G et al (2020) Investigating serum and tissue expression identified a cytokine/chemokine signature as a highly effective melanoma marker. *Cancers* 12: 3680
- Chomczynski P, Sacchi N (1987) Single-step method of RNA isolation by acid guanidinium thiocyanate-phenol-chloroform extraction. *Anal Biochem* 162: 156–159
- Coffelt SB, Kersten K, Doornebal CW, Weiden J, Vrijland K, Hau CS, Versteegen NJM, Ciampricotti M, Hawinkels L, Jonkers J et al (2015) IL-17-producing gammadelta T cells and neutrophils conspire to promote breast cancer metastasis. *Nature* 522: 345–348
- Coussens LM, Werb Z (2002) Inflammation and cancer. *Nature* 420: 860–867
- Coutelle O, Hornig-Do H-T, Witt A, Andree M, Schiffmann LM, Piekarek M, Brinkmann K, Seeger JM, Liwschitz M, Miwa S et al (2014) Embelin inhibits endothelial mitochondrial respiration and impairs neoangiogenesis during tumor growth and wound healing. *EMBO Mol Med* 6: 624–639
- Cummins JM, Kohli M, Rago C, Kinzler KW, Vogelstein B, Bunz F (2004) X-linked inhibitor of apoptosis protein (XIAP) is a nonredundant modulator of tumor necrosis factor-related apoptosis-inducing ligand (TRAIL)-mediated apoptosis in human cancer cells. *Cancer Res* 64: 3006–3008
- Damgaard R, Nachbur U, Yabal M, Wong W-L, Fiil B, Kastirr M, Rieser E, Rickard J, Bankovacki A, Peschel C et al (2012) The ubiquitin ligase XIAP recruits LUBAC for NOD2 signaling in inflammation and innate immunity. *Mol Cell* 46: 746–758
- Eckelman BP, Salvesen GS, Scott FL (2006) Human inhibitor of apoptosis proteins: why XIAP is the black sheep of the family. *EMBO Rep* 7: 988–994
- Emanuel PO, Phelps RG, Mudgil A, Shafir M, Burstein DE (2008) Immunohistochemical detection of XIAP in melanoma. *J Cutan Pathol* 35: 292–297
- Farahani R, Fong WG, Korneluk RG, MacKenzie AE (1997) Genomic organization and primary characterization of miap-3: the murine homologue of human X-linked IAP. *Genomics* 42: 514–518
- Fritsch M, Günther SD, Schwarzer R, Albert M-C, Schorn F, Werthenbach JP, Schiffmann LM, Stair N, Stocks H, Seeger JM et al (2019) Caspase-8 is the molecular switch for apoptosis, necroptosis and pyroptosis. *Nature* 575: 683–687
- Fulda S, Vucic D (2012) Targeting IAP proteins for therapeutic intervention in cancer. *Nat Rev Drug Discov* 11: 109–124
- Giebeler N, Schonefuss A, Landsberg J, Tuting T, Mauch C, Zigrino P (2017) Deletion of ADAM-9 in HGF/CDK4 mice impairs melanoma development and metastasis. *Oncogene* 36: 5058–5067
- Goncharov T, Hedayati S, Mulvihill MM, Izrael-Tomasevic A, Zobel K, Jeet S, Fedorova AV, Eidschenk C, deVoss J, Yu K et al (2018) Disruption of XIAP-RIP2 association blocks NOD2-mediated inflammatory signaling. *Mol Cell* 69: 551–565
- Gregory AD, Houghton AM (2011) Tumor-associated neutrophils: new targets for cancer therapy. *Cancer Res* 71: 2411–2416
- Günther SD, Fritsch M, Seeger JM, Schiffmann LM, Snipas SJ, Coutelle M, Kufer TA, Higgins PG, Hornung V, Bernardini ML et al (2020) Cytosolic Gram-negative bacteria prevent apoptosis by inhibition of effector caspases through lipopolysaccharide. *Nat Microbiol* 5: 354–367
- Hanahan D, Weinberg RA (2011) Hallmarks of cancer: the next generation. *Cell* 144: 646–674
- Harlin H, Reffey SB, Duckett CS, Lindsten T, Thompson CB (2001) Characterization of XIAP-deficient mice. *Mol Cell Biol* 21: 3604–3608
- Hasegawa M, Fujimoto Y, Lucas PC, Nakano H, Fukase K, Nunez G, Inohara N (2008) A critical role of RICK/RIP2 polyubiquitination in Nod-induced NF-kappaB activation. *EMBO J* 27: 373–383
- Heim VJ, Dagley LF, Stafford CA, Hansen FM, Clayer E, Bankovacki A, Webb AI, Lucet IS, Silke J, Nachbur U (2020) A regulatory region on RIPK2 is required for XIAP binding and NOD signaling activity. *EMBO Rep* 21: e50400
- Hiscutt EL, Hill DS, Martin S, Kerr R, Harbottle A, Birch-Machin M, Redfern CP, Fulda S, Armstrong JL, Lovat PE (2010) Targeting X-linked inhibitor of apoptosis protein to increase the efficacy of endoplasmic reticulum stress-induced apoptosis for melanoma therapy. *J Invest Dermatol* 130: 2250–2258
- Hofer-Warbinek R, Schmid JA, Stehlik C, Binder BR, Lipp J, de Martin R (2000) Activation of NF-kappa B by XIAP, the X chromosome-linked inhibitor of apoptosis, in endothelial cells involves TAK1. *J Biol Chem* 275: 22064–22068
- Hornle M, Peters N, Thayaparasingham B, Vorsmann H, Kashkar H, Kulms D (2011) Caspase-3 cleaves XIAP in a positive feedback loop to sensitize melanoma cells to TRAIL-induced apoptosis. *Oncogene* 30: 575–587
- Hrdinka M, Schlicher L, Dai B, Pinkas DM, Bufton JC, Picaud S, Ward JA, Rogers C, Suebsuwong C, Nikhar S et al (2018) Small molecule inhibitors reveal an indispensable scaffolding role of RIPK2 in NOD2 signaling. *EMBO J* 37: e99372
- Jensen TO, Schmidt H, Moller HJ, Donskov F, Hoyer M, Sjoegren P, Christensen IJ, Steiniche T (2012) Intratumoral neutrophils and plasmacytoid dendritic cells indicate poor prognosis and are associated with pSTAT3 expression in AJCC stage I/II melanoma. *Cancer* 118: 2476–2485
- Kashkar H (2010) X-linked inhibitor of apoptosis: a chemoresistance factor or a hollow promise. *Clin Cancer Res* 16: 4496–4502
- Krieg A, Correa RG, Garrison JB, Le Negrate G, Welsh K, Huang Z, Knoefel WT, Reed JC (2009) XIAP mediates NOD signaling via interaction with RIP2. *Proc Natl Acad Sci USA* 106: 14524–14529
- Lecis D, Drago C, Manzoni L, Seneci P, Scolastico C, Mastrangelo E, Bolognesi M, Anichini A, Kashkar H, Walczak H et al (2010) Novel SMAC-mimetics synergistically stimulate melanoma cell death in combination with TRAIL and Bortezomib. *Br J Cancer* 102: 1707–1716
- Listen P, Roy N, Tamai K, Lefebvre C, Baird S, Cherton-Horvat G, Farahani R, McLean M, Ikeda J-E, Mackenzie A et al (1996) Suppression of apoptosis in mammalian cells by NAIP and a related family of IAP genes. *Nature* 379: 349–353
- Lu M, Lin SC, Huang Y, Kang YJ, Rich R, Lo YC, Myszka D, Han J, Wu H (2007) XIAP induces NF-kappaB activation via the BIR1/TAB1 interaction and BIR1 dimerization. *Mol Cell* 26: 689–702
- Mantovani A, Sica A, Allavena P, Garlanda C, Locati M (2009) Tumor-associated macrophages and the related myeloid-derived suppressor cells as a paradigm of the diversity of macrophage activation. *Hum Immunol* 70: 325–330

- Masucci MT, Minopoli M, Carriero MV (2019) Tumor associated neutrophils. Their role in tumorigenesis, metastasis, prognosis and therapy. *Front Oncol* 9: 1146
- Nachbur U, Stafford CA, Bankovacki A, Zhan Y, Lindqvist LM, Fiil BK, Khakham Y, Ko H-J, Sandow JJ, Falk H et al (2015) A RIPK2 inhibitor delays NOD signalling events yet prevents inflammatory cytokine production. *Nat Commun* 6: 6442
- Nakatani Y, Kleffmann T, Linke K, Condon SM, Hinds MG, Day CL (2013) Regulation of ubiquitin transfer by XIAP, a dimeric RING E3 ligase. *Biochem J* 450: 629–638
- Payne AS, Cornelius LA (2002) The role of chemokines in melanoma tumor growth and metastasis. *J Invest Dermatol* 118: 915–922
- Prakash H, Albrecht M, Becker D, Kuhlmann T, Rudel T (2010) Deficiency of XIAP leads to sensitization for Chlamydomydia pneumoniae pulmonary infection and dysregulation of innate immune response in mice. *J Biol Chem* 285: 20291–20302
- Ramakers C, Ruijter JM, Deprez RH, Moorman AF (2003) Assumption-free analysis of quantitative real-time polymerase chain reaction (PCR) data. *Neurosci Lett* 339: 62–66
- Schiffmann LM, Fritsch M, Gebauer F, Günther SD, Stair NR, Seeger JM, Thangarajah F, Dieplinger G, Bludau M, Alakus H et al (2019) Tumour-infiltrating neutrophils counteract anti-VEGF therapy in metastatic colorectal cancer. *Br J Cancer* 120: 69–78
- Schiffmann LM, Werthenbach JP, Heintges-Kleinhofer F, Seeger JM, Fritsch M, Günther SD, Willenborg S, Brodesser S, Lucas C, Jüngst C et al (2020) Mitochondrial respiration controls neoangiogenesis during wound healing and tumour growth. *Nat Commun* 11: 3653
- Seeger JM, Brinkmann K, Yazdanpanah B, Haubert D, Pongratz C, Coutelle O, Kronke M, Kashkar H (2010a) Elevated XIAP expression alone does not confer chemoresistance. *Br J Cancer* 102: 1717–1723
- Seeger JM, Schmidt P, Brinkmann K, Hombach AA, Coutelle O, Zigrino P, Wagner-Stippich D, Mauch C, Abken H, Krönke M et al (2010b) The proteasome inhibitor bortezomib sensitizes melanoma cells toward adoptive CTL attack. *Cancer Res* 70: 1825–1834
- Silke J, Vucic D (2014) IAP family of cell death and signaling regulators. *Methods Enzymol* 545: 35–65
- Soengas MS, Lowe SW (2003) Apoptosis and melanoma chemoresistance. *Oncogene* 22: 3138–3151
- Szczerba BM, Castro-Giner F, Vetter M, Krol I, Gkoutela S, Landin J, Scheidmann MC, Donato C, Scherrer R, Singer J et al (2019) Neutrophils escort circulating tumour cells to enable cell cycle progression. *Nature* 566: 553–557
- Takeda AN, Oberoi-Khanuja TK, Glatz G, Schulenburg K, Scholz RP, Carpy A, Macek B, Remenyi A, Rajalingam K (2014) Ubiquitin-dependent regulation of MEKK2/3-MEK5-ERK5 signaling module by XIAP and cIAP1. *EMBO J* 33: 1784–1801
- Tormo D, Ferrer A, Gaffal E, Wenzel J, Basner-Tschakarjan E, Steitz J, Heukamp LC, Gütgemann I, Buettner R, Malumbres M et al (2006) Rapid growth of invasive metastatic melanoma in carcinogen-treated hepatocyte growth factor/scatter factor-transgenic mice carrying an oncogenic CDK4 mutation. *Am J Pathol* 169: 665–672
- Uren AG, Pakusch M, Hawkins CJ, Puls KL, Vaux DL (1996) Cloning and expression of apoptosis inhibitory protein homologs that function to inhibit apoptosis and/or bind tumor necrosis factor receptor-associated factors. *Proc Natl Acad Sci USA* 93: 4974–4978
- Varfolomeev E, Vucic D (2008) (Un)expected roles of c-IAPs in apoptotic and NFkappaB signaling pathways. *Cell Cycle* 7: 1511–1521
- Witt A, Seeger JM, Coutelle O, Zigrino P, Broxtermann P, Andree M, Brinkmann K, Jungst C, Schauss AC, Schull S et al (2015) IAP antagonization promotes inflammatory destruction of vascular endothelium. *EMBO Rep* 16: 719–727
- Yamaguchi K, Nagai S, Ninomiya-Tsuji J, Nishita M, Tamai K, Irie K, Ueno N, Nishida E, Shibuya H, Matsumoto K (1999) XIAP, a cellular member of the inhibitor of apoptosis protein family, links the receptors to TAB1-TAK1 in the BMP signaling pathway. *EMBO J* 18: 179–187
- Yang Y, Fang S, Jensen JP, Weissman AM, Ashwell JD (2000) Ubiquitin protein ligase activity of IAPs and their degradation in proteasomes in response to apoptotic stimuli. *Science* 288: 874–877



**License:** This is an open access article under the terms of the Creative Commons Attribution-NonCommercial-NoDeriv License, which permits use and distribution in any medium, provided the original work is properly cited, the use is non-commercial and no modifications or adaptations are made.